EUROPEAN ORGANIZATION FOR NUCLEAR RESEARCH

CERN-EP/84-80
6 July 1984

THE $\rho'(1600)$ IN THE REACTION $\gamma p \to \pi^+\pi^-\pi^0\pi^0 p$ AT PHOTON ENERGIES OF 20-70 GeV

The Omega Photon Collaboration

M. Atkinson[7], T.J. Axon[5], D. Barberis[5], T.J. Brodbeck[4], G.R. Brookes[8], J.J. Bunn[8], P.J. Bussey[3], A.B. Clegg[4], J.B. Dainton[3], M. Davenport[7], B. Dickinson[5], B. Diekmann[1], A. Donnachie[5], R.J. Ellison[5], P. Flower[7], P.J. Flynn[4], W. Galbraith[8], K. Heinloth[1], R.C.W. Henderson[4], R.E. Hughes-Jones[5], J.S. Hutton[7], M. Ibbotson[5], H.-P. Jakob[1], M. Jung[1], B.R. Kumar[7], J. Laberrigue[6], G.D. Lafferty[5], J.B. Lane[5], J.-C. Lassalle[2], J.M. Lévy[6], V. Liebenau[1], R. McClatchey[8], D. Mercer[5], J.A.G. Morris[7], J.V. Morris[7], D. Newton[4], C. Paterson[3], G.N. Patrick[2], E. Paul[1], C. Raine[3], M. Reidenbach[1], H. Rotscheidt[1], A. Schlösser[1], P.H. Sharp[7], I.O. Skillicorn[3], K.M. Smith[3], K.M. Storr[2], R.J. Thompson[5], Ch. de la Vaissière[6], A.P. Waite[5], M.F. Worsell[5] and T.P. Yiou[6]

Bonn[1]-CERN[2]-Glasgow[3]-Lancaster[4]-Manchester[5]-Paris VI[6]-Rutherford[7]-Sheffield[8]

ABSTRACT

The reaction $\gamma p \to \pi^+\pi^-\pi^0\pi^0 p$ (excluding $\omega\pi^0$ production) has been studied for photon energies in the range 20-70 GeV. A peak is seen in the 4π mass spectrum at ~ 1.66 GeV with a width of ~ 0.3 GeV which is identified with the $\rho'(1600)$. Maximum likelihood fits show that the peak is dominantly in $\rho^{\pm}\pi^{\mp}\pi^0$ with $B(\rho' \to \rho^0\pi^0\pi^0)/B(\rho' \to \rho^{\pm}\pi^{\mp}\pi^0) < 0.1$. This indicates an $I = 1$ $\rho\pi$ final-state interaction. However, no evidence is found for any resonant $\rho\pi$ state such as an A_1 or π'.

(To be submitted to Zeitschrift für Physik C)

0004P/RJE/sm

1. INTRODUCTION

The $\rho'(1600)$ has previously been observed in the decay modes $\pi^+\pi^-\pi^+\pi^-$, [1-5] $\pi^+\pi^-\pi^0\pi^0$ [6,7], $\pi^+\pi^-$ [8,9] and possibly $\eta\pi^+\pi^-$ [10]. A detailed analysis of the reaction $\gamma p \to \pi^+\pi^-\pi^+\pi^- p$ in the same energy range as used in the present experiment, has been reported[2].

The study of the ρ' in the channel

$$\gamma p \to \rho' p \to \pi^+\pi^-\pi^0\pi^0 p \qquad (1)$$

is of interest because the ratio of charged to neutral ρ-meson production is different for different ρ'decay schemes. For example in the case of $\rho' \to \rho\varepsilon$ the decay would be to ρ^0 with the $\pi^0\pi^0$ system in a relative s-wave, while for $\rho' \to A_1\pi$ or $\pi'\pi$ [11], the decay would be to $\rho^\pm\pi^\mp\pi^0$. The analysis of $\rho' \to \pi^+\pi^-\pi^+\pi^-$ was unable to distinguish between these possibilities[2] while a previous study of reaction (1) has shown[6] the dominance of $\rho^\pm$ over ρ^0 in the data. This suggests a decay of the ρ'through an I = 1 intermediate $\rho\pi$ state. There is however still much uncertainty about the nature of I = 1 states decaying to 3π. The A_1 has been reported with a wide range of parameters[12] and the π' has been reported with a very large uncertainty in its width and with little evidence for $\rho\pi$ as a decay mode[13]. The alternative explanation for a dominance of $\rho^\pm$ over ρ^0 would be the occurrence of a strong $\rho\rho$ decay mode of the ρ', which cannot contribute to $\pi^+\pi^-\pi^+\pi^-$ and so would require the $\gamma p \to \pi^+\pi^-\pi^0\pi^0 p$ cross-section to be larger than $\gamma p \to \pi^+\pi^-\pi^+\pi^- p$ in the ρ' region.

This paper reports on a detailed analysis of reaction (1) from an experiment (WA57) on the CERN SPS. A preliminary analysis has been reported previously[6].

2. EXPERIMENTAL SET-UP

A photon beam, tagged in the energy range 20-70 GeV to an accuracy of ~ 150 MeV, was produced by bremsstrahlung from an 80 GeV (±2%) electron beam[14] at the CERN SPS. The photons entered the Omega spectrometer which was equipped with a 60 cm long liquid hydrogen target, multiwire proportional chambers and, downstream of the magnet, drift chambers (DC1, DC2), a threshold Cherenkov counter and a photon detector. The layout is shown

in Fig. 1. The photon calorimeter was made up of an active converter of 42 slabs of lead glass, each three radiation lengths deep, followed by a shower position detector hodoscope of 792 scintillation counters and, finally, an array of 343 lead glass blocks, each of an area 140 x 140 mm^2 and 20 radiation lengths in depth. This calorimeter covered a solid angle of 0.07 steradian about the forward direction and measured photon direction and energy to ±0.4 mrad and ±0.10 $E^{1/2}$ GeV, respectively.

The trigger for reaction (1) required two to five forward charged particles together with a signal indicating at least one γ-ray of energy greater than 2 GeV in the photon detector. A system of veto counters in the median plane was used to reduce the background from electromagnetic processes to a level well below the hadronic trigger rate. A total of ~ 10^7 events was recorded.

3. DATA REDUCTION AND SIMULATION

The events were processed through an analysis chain consisting of a pattern recognition and vertex finding programme for charged tracks [TRIDENT[15)]], an incident photon reconstruction programme, a charged particle identification programme and a secondary photon and π^o reconstruction programme. Reaction (1) was selected by requiring two reconstructed π^o's and two or three charged tracks (originating from a vertex in the target) of which one was negatively charged. If two positively charged tracks were found, one had to be consistent in momentum and angle with being a recoil proton from reaction (1). The longitudinal momentum difference between the tagged photon and the observed particles was required to be less than 1.5 GeV.

The events due to ωπ production have been reported previously[16)]. Hence, here, events have been rejected if either of the two $\pi^+\pi^-\pi^o$ combinations had an effective mass in the range $0.74 < M_{\pi^+\pi^-\pi^o} < 0.84$ GeV. (This applies to all plots with the exception of Fig. 3a.) Although this cut affects the acceptance for low 4π masses, it only rejects a small fraction of non-ω events in the mass range of the ρ'.

The Cherenkov counter was able to distinguish pions from kaons and protons in the momentum range 5.6 to 18.6 GeV/c whereas the single particle momentum spectrum peaks below this range. Most kaons are therefore not

identified and so, to simplify the simulation, the Cherenkov counter information was ignored. Thus all charged particles were assumed to be pions with the exception of those identified from angle measurements as recoil protons. The difference in longitudinal momentum between the incident photon and the detected particles (see Fig. 2a) was used to estimate the background contribution of events with further, undetected, particles at less than 15%.

The analysis required a sample of simulated events that passed the trigger and analysis programmes both for original identification of particles and for the cuts on events. The Monte Carlo simulation of the experiment was carried out by generating 4π phase-space events, using the programme SAGE[17] with an appropriate incident γ spectrum, t distribution, and $\pi^+\pi^-\pi^0\pi^0$ effective mass distribution. The 4π effective mass and t distribution for the simulation were chosen so that the final distributions of these parameters after the acceptance programme matched those for the experimental data. The simulated events were processed through the appropriate parts of the analysis programmes and the effects of the detector resolution were folded in. In particular, for the π^0 detection, a Monte Carlo programme was used to simulate showering and the events were reconstructed with the same programme as was used for the real data. Some resulting distributions from the simulation are shown in Fig. 2 together with the corresponding distributions for the data. In order to get information on acceptance for events from particular processes, e.g. $\gamma p \to \rho^+\pi^-\pi^0 p$, the simulated events were weighted with the appropriate decay intensities as discussed in Section 5.

4. GENERAL FEATURES OF THE DATA

Figure 3 shows the measured $\pi^+\pi^-\pi^0\pi^0$ mass spectrum both before and after the ω exclusion described in Section 3. The main feature of the mass spectrum, after ω exclusion, is a peak at $M_{4\pi} \sim 1.6$ GeV which is naturally identified with the $\rho'(1600)$. [Some admixture of the g(1670) cannot be excluded, but the absence of a strong $A_2\pi$ signal (see below) is evidence against a dominant g(1670) [18].] The t distribution (not shown) indicates peripheral production with an exponential t dependence of exponent 5.5 ± 0.2 $(\mathrm{GeV}/c^2)^2$. Figures 4a-4c show the $\pi^+\pi^-$, $\pi^\pm\pi^0$ and $\pi^0\pi^0$ mass spectra for events satisfying the cut $1.4 < M_{4\pi} < 1.8$ GeV. The curves are the appropriate simulated distributions resulting from 4π

phase space. The large amount of $\rho^{\pm}$ (an average of 2/3 of a charged ρ per event) and the absence of a clear ρ^{o} peak shows that the dominant decay of the 1.6 GeV peak is to $\rho^{\pm}\pi^{+}\pi^{o}$ rather than to $\rho^{o}\pi^{o}\pi^{o}$. Natural explanations for this are an I = 1 $\rho\pi$ final-state interaction or a $\rho^{+}\rho^{-}$ decay mode for the ρ'.

The measured $\pi^{+}\pi^{-}\pi^{o}$ and $\pi^{\pm}\pi^{o}\pi^{o}$ mass spectra (Figs. 4d, 4e) both show a width which is close to that of the simulation assuming $\rho^{\pm}\pi^{+}\pi^{o}$ phase space (solid curve). Any resonant $\rho\pi$ final state interaction, such as A_1 or π', would be expected to show up as a narrowing of the $\pi^{\pm}\pi^{o}\pi^{o}$ mass distribution for data relative to this simulation. There is no indication of such narrowing, showing that if the dominant decay of the ρ' is via $A_1^{\pm}\pi^{\mp}$ or $\pi'^{\pm}\pi^{+}$, then the A_1 or π' must be broad ($\geq$ 700 MeV). The $\pi^{\pm}\pi^{o}\pi^{o}$ mass spectrum shows a slight excess at 1.3 GeV compatible with a small A_2 contribution to the process.

The relevant angular distributions of various particles are, in general, flat and do not differ strongly from those given by the phase space simulation. For the decay of the $\rho'(1600)$ via $\pi^{+}\pi^{-}\pi^{+}\pi^{-}$, the $\pi^{+}\pi^{+}$ (or $\pi^{-}\pi^{-}$) direction in the 4π cm system is a good analyser of the spin alignment of the 4π state because of the requirement of Bose symmetry of these $\pi\pi$ pairs[19]. The $\pi^{o}\pi^{o}$ direction is an analogous analyser for the decay $\rho'(1600) \to \pi^{+}\pi^{-}\pi^{o}\pi^{o}$ but it is much inferior both because its efficiency falls more rapidly with increasing mass and because it is significantly affected by the π^{o} acceptance.

5. MAXIMUM LIKELIHOOD FITS

To get further information more detailed analyses were carried out guided by the general features noted in the previous section. In general the problem can be studied by an extension of the angular momentum analysis techniques due to Zemach[20] but the number of independent free parameters is too large to be constrained by the data. Hence maximum likelihood fits have been made with many simplifying assumptions. The maximum likelihood technique[21] used the data and the Monte Carlo simulation discussed in (3) to evaluate likelihoods and the programme MINUIT[22] to minimize the negative log likelihood and hence find best estimates for the various contributions.

All fits were performed in 100 MeV wide bins of 4π mass with no constraints on smooth behaviour between bins. Masses and widths for resonant states have been taken from the Particle Data Tables[23] for all states except the ρ meson where an improvement in the fit was obtained with a mass of 785 MeV [2].

Since there is a contribution to the data which does not contain $\rho^{\pm}$, all fits have included a contribution from 4π phase space. A further possible contribution to the non-$\rho^{\pm}$ events is $\rho^{o}\pi^{o}\pi^{o}$ phase space and such a contribution was included in some fits. The $\pi^{o}\pi^{o}$ mass plot shows a background contribution (of ~ 10%) from $K^{o} \to \pi^{o}\pi^{o}$ which was parametrized in all fits by $\gamma p \to K^{*}Kp$ followed by $K^{*} \to K\pi^{\pm}$. (The $K^{\mp}$ is recontructed as a $\pi^{\mp}$ and the K^{o} decays to $\pi^{o}\pi^{o}$ to fake the event selection.)

The $\rho^{\pm}\pi^{\mp}\pi^{o}$ contribution has been studied both in terms of angular momentum of pairs of particles and in terms of specific resonant intermediate states.

i) Using the angles and angular momenta defined in Fig. 5 where θ_{ρ} and $\theta_{\pi\pi}$ are measured in the rest frames of the $\pi\pi$ pairs, the need for any values of ℓ and L higher than 0 has been studied. The $\ell = L = 0$ matrix element is independent of θ_{ρ} and $\theta_{\pi\pi}$. If either or both ℓ and L are 1 then the position is more complicated. As an exploration a fit has been done allowing terms linear in each of the scalars readily constructed from the momentum vectors viz

$$M = \sum_{i=1}^{4} \frac{\sin \delta_i}{q^2} \exp(i\delta_i)(A + B\hat{p}_{\rho}\cdot\hat{\phi}_{\pi^0_1} + C\hat{p}_{\pi\pi}\cdot\hat{p}_{\pi^0_2} + D\hat{p}_{\pi^0_1}\cdot\hat{p}_{\pi^0_2})$$

$$= \sum_{i=1}^{4} \frac{\sin \delta_i}{q^2} \exp(i\phi_i)[A + B\cos\theta_{\rho} + C\cos\theta_{\pi\pi} + D(\cos\theta_{\rho}\cos\theta_{\pi\pi} + \sin\theta_{\rho}\sin\theta_{\pi\pi}\cos\phi)]$$

where δ_i are the p wave π-π phase shifts for the pair forming the ρ, ϕ is the azimuthal angle between the "$\pi\pi$" and "ρ" decay planes, q is the

momentum of either π in the ρ rest system and the sum is over the four possible identifications of the ρ. A, B, C, and D have been taken to be real. This form includes contributions from orbital angular momenta up to 1 but is not completely general. This matrix element squared was then added to a 4π phase space intensity and a $K^0_S K^{\pm}\pi^{\mp}$ contribution as discussed above.

ii) A range of phase-space contributions through specific states have been tried. These were $\rho^{\pm}\pi^{+}\pi^{0}$, $A_1^{\pm}\pi$ (followed by $A_1^{\pm} \to \rho^{\pm}\pi^{0}$), $\pi'^{\pm}\pi^{\mp}$ (followed by $\pi'^{\pm} \to \rho^{\pm}\pi^{0}$), $H\pi^{0}$ (followed by $H \to \rho\pi$), and $\rho^{+}\rho^{-}$. All resonance contributions are parametrized as final state interaction amplitudes and different assignments of particles to a resonance are added correctly as amplitudes before squaring (see Appendix of Ref. 2). The reaction may proceed through an s-channel helicity conserving mechanism (SCHC) and contributions with either SCHC alignment or isotropy were used. In addition a contribution for $A_2^{\pm}\pi^{\mp}$ (followed by $A_2^{\pm} \to \rho^{\pm}\pi^{0}$) was allowed because of the indications of an A_2 peak in the data. The above contributions were fitted only as individual intensities. The number of free parameters allowing for all possible interference terms is too large to be constrained by the data.

The results of analysing the $\rho^{\pm}\pi^{\mp}\pi^{0}$ contribution in terms of angular momenta of pairs of particles is shown in Fig. 6. The errors on the numbers of events in each contribution are those given by MINUIT. The only significant $\rho^{\pm}\pi^{\mp}\pi^{0}$ intensity is seen to be isotropic, corresponding to $L = \ell = 0$ (Fig. 6a) and to be strongly peaked at a mass $\sim$ 1.68 GeV with a width $\sim$ 0.3 GeV. Figures 7a to 7e show as examples the data and the results of the fit for the mass spectra $\pi^{+}\pi^{-}$, $\pi^{\pm}\pi^{0}$, $\pi^{0}\pi^{0}$, $\pi^{+}\pi^{-}\pi^{0}$, and $\pi^{\pm}\pi^{0}\pi^{0}$, respectively, for the 4π mass range 1.6 to 1.7 GeV. The fits to these mass spectra are acceptable and there is no evidence that any non-zero internal orbital angular momenta between the final $\rho^{\pm}$, $\pi^{\mp}$, and π^{0} are needed to fit the data.

As an example the intensities determined from fits using one specific set of resonance contributions are shown in Fig. 8. The contribution assumed for this example are a combination of isotropically aligned phase space models of $\rho^{0}\pi^{0}\pi^{0}$, $\rho^{\pm}\pi^{\mp}\pi^{0}$, $A_1^{\pm}\pi^{\mp}$, $A_2^{\pm}\pi^{\mp}$, $\rho^{+}\rho^{-}$, $H^{0}\pi^{0}$, $\pi'^{\pm}\pi^{\mp}$, $\pi^{+}\pi^{-}\pi^{0}\pi^{0}$ plus the $K^0_S K^{\pm}\pi^{\mp}$ background. In practice these fits are not significantly better than those leading to Fig. 6, thus showing that the data do not need as many

free parameters in order to fit it as are allowed. In particular because different contributions can have very similar distributions, particularly just above their threshold, some instability in the fit parameters as a function of 4π mass is expected. There are, however, certain conclusions that can be drawn from this fit, and from similar fits with various combinations of resonance contributions. The dominance of $\rho^{\pm}\pi^{\mp}\pi^{o}$ over $\rho^{o}\pi^{o}\pi^{o}$ is always found. The $\rho^{o}\pi^{o}\pi^{o}$ phase space contribution, Fig. 8f, is both small and largely non-resonant with a ratio $B(\rho^{o}\pi^{o}\pi^{o})/B(\rho^{\pm}\pi^{\mp}\pi^{o}) < 0.1$ thus excluding a dominant decay of the 4π resonance via a neutral ρ^{o} state. The $\rho\rho$ contribution (Fig. 8g) also shows no resonant structure and could well be an artifact due to the effective mass of a phase space $\pi\pi$ system recoiling against a $\rho^{\pm}$ being peaked in the ρ mass region. All fits show that $\rho^{\pm}\pi^{\mp}\pi^{o}$, a 4π phase space contribution varying slowly with 4π mass and a $KK\pi$ background, are the only contributions that are essential to fit the data. Another general result from these fits is that, despite the obvious explanation for the dominance of $\rho^{\pm}\pi^{\mp}\pi^{o}$ being a strong $\rho\pi$ final state interaction, there is no evidence for a resonant π' contribution or for any relatively narrow A_1. Whether the parameters assumed for the A_1 are those given by the Particle Data Group[21] (as assumed in Fig. 8) or the modified parameters which gave an improved fit to the $\rho' \to \pi^{+}\pi^{-}\pi^{+}\pi^{-}$ decay[2], the fit always chooses $\rho^{\pm}\pi^{\mp}\pi^{o}$ phase space rather than $A_1\pi$.

In order to understand further the results of the fits, acceptance corrected Monte Carlo mass spectra for each of the contributions are compared with data. Figure 9a shows the $\pi^{\pm}\pi^{o}\pi^{o}$ mass spectra calculated from the simulation for $A_1\pi$ (solid line), and $\rho^{\pm}\pi^{\mp}\pi^{o}$ phase space (dotted line). The $A_1\pi$ spectrum (taking Particle Data Tables parameters for the A_1), shows a width ~ 330 MeV, which is seen to be considerably narrower than the ~ 450 GeV of the $\rho^{\pm}\pi^{\mp}\pi^{o}$ phase space spectrum. The $\pi^{\pm}\pi^{o}\pi^{o}$ mass spectrum for the data (Fig. 7e) is similar in width to the latter. Distributions for $\rho^{\pm}\pi^{\mp}\pi^{o}$ phase space and an $A_1\pi$ process are clearly very similar if the width of the A_1 is very large. In practice the data are unable to distinguish between the two if the width of the A_1 is greater than ~ 700 MeV. The explanation in terms of a wide π' is excluded by the shape of the $\rho^{\pm}\pi^{\mp}\pi^{o}$ Dalitz plot distribution which favours the $\rho\pi$ being in a $J^{P} = 1^{+}$ rather than a 0^{-} state.

Since SCHC alignment in the production of the ρ' has been reported[1,2,8] this possibility has been considered by fitting the contributions $\rho^{\pm}\pi^{\mp}\pi^{o}$, $A_1^{\pm}\pi^{\mp}$ and $\pi'^{\pm}\pi^{\mp}$ with SCHC alignment. Such fits were less good than for an unaligned state; a notable difference is in the $\pi^{\pm}\pi^{o}$ mass spectra shown in Fig. 9b where the $\rho^{\pm}\pi^{\mp}\pi^{o}$ is shown with SCHC alignment (solid line) and with isotropy (dotted line). The shape of the mass spectrum for the data (Fig. 7b) closely resembles that of the Monte Carlo results for isotropic alignment. While the SCHC alignment fails to reproduce this 2π mass spectrum the lack of a direct sensitive analyser somewhat weakens the argument for a non-SCHC mechanism since it is conceivable that some other effect could perturb the 2π mass spectrum and perhaps alter the result of the fit procedure.

The cross-section for production of $\rho^{\pm}$ in 4π systems of mass below 1.8 GeV was found to be 600 ± 200 nb (the error is dominantly systematic). This can be compared with the cross-section of 590 ± 170 nb for the corresponding production of $\rho^{o}\pi^{+}\pi^{-}$ deduced from a previous experiment[2]. The agreement between these two cross-sections is consistent with the corresponding agreement between $\pi^{+}\pi^{-}\pi^{+}\pi^{-}$ [3-5] and $\pi^{+}\pi^{-}\pi^{o}\pi^{o}$ [7] production cross-sections measured in electron-positron annihilations.

5. DISCUSSION OF RESULTS AND CONCLUSIONS

A peak has been seen in the $\pi^{+}\pi^{-}\pi^{o}\pi^{o}$ effective mass distribution of reaction (1). The enhancement decays dominantly via $\rho^{\pm}\pi^{\mp}\pi^{o}$ with

$$\frac{B(\rho' \to \rho^{o}\pi^{o}\pi^{o})}{B(\rho' \to \rho^{\pm}\pi^{\mp}\pi^{o})} < 0.1 \ .$$

and implies either that the $\rho\pi$ is in an I = 1 state or that the decay is to $\rho^{+}\rho^{-}$. On the former hypothesis, which was also allowed by the $\pi^{+}\pi^{-}\pi^{+}\pi^{-}$ analysis[2], one might expect to see some manifestation of a π' or A_1. On the basis of the present analysis, which neglects interference between amplitudes, the $\pi'\pi$ interpretation cannot dominate while the $A_1\pi$ interpretation can only dominate if the width of the A_1 is $\gtrsim 0.7$ GeV. The similarity of cross-sections for $\rho^{\pm}\pi^{\mp}\pi^{o}$ and $\rho^{o}\pi^{+}\pi^{-}$ also fits in with the $A_1\pi$ hypothesis. [A broad A_1 would not conflict with the $\pi^{\pm}\pi^{+}\pi^{-}$ spectra for the $\rho^{o}\pi^{+}\pi^{-}$ process[2] but some additional effect would have to be added to the interpretation to explain the 2π spectra seen in that experiment.] The $\rho\rho$ hypothesis raises two difficulties; the production cross-section for

$\rho^{\pm}\pi^{\mp}\pi^{o}$ is not substantially larger than for $\rho^{o}\pi^{+}\pi^{-}$ (to which $\rho\rho$ cannot contribute) and the fits, while allowing some $\rho^{+}\rho^{-}$ contribution, show no sign of a resonance and give little improvement in the probability of the fit.

The peak in the $\pi^{+}\pi^{-}\pi^{o}\pi^{o}$ mass spectrum is at ~ 1.65 GeV, while fits in which a 4π phase space background was included together with a $\rho^{\pm}\pi^{\mp}\pi^{o}$ contribution gave a peak in the $\rho^{\pm}\pi^{\mp}\pi^{o}$ intensity at a higher mass ~ 1.68 GeV and a range of widths. From this range of results our best estimate of the mass of the peak is 1.66 ± 0.03 GeV and of its width is 0.30 ± 0.05 GeV. These values are to be compared with measurements of other decay modes observed in photoproduction.

Channel	Mass	Width	Reference
$\rho^{o}\pi^{+}\pi^{-}$	1.52 ± 0.03	0.40 ± 0.05	2
$\pi^{+}\pi^{-}$	1.60 ± 0.01	0.28 ± 0.01	8
	1.59 ± 0.02	0.23 ± 0.08	9

Agreement in $\rho'(1600)$ peaks in $\pi^{+}\pi^{-}\pi^{+}\pi^{-}$ between photoproduction and electron-positron annihilation has been noted previously[2]. The high mass value found in $\rho^{\pm}\pi^{\mp}\pi^{o}$ could be interpreted as showing a major contribution of the g(1670) to this channel, with the lower mass in $\rho^{o}\pi^{+}\pi^{-}$ implying suppression of g(1670) in that charge state. Such an interpretation is inconsistent with the agreement in cross-sections between the two charge states and the weakness, reported here, of decay modes (such as $\rho^{+}\rho^{-}$) that could lead to the suppression. A further argument is the lack of $A_2\pi$ which is reported[18,21] to be a substantial fraction (~ 0.5) of the 4π decay mode of the g.

A third problem in reconciling results for the different channels is the indication of isotropy in the $\rho^{\pm}\pi^{\mp}\pi^{o}$ and the indications of SCHC alignment in the other two states[1,2,9].

These three problems show that, the situation is more complicated than the traditional interpretation in terms of a single $\rho'(1600)$ together with a non-interfering background. The most likely explanations appear to be either strong interference effects between the $\rho'(1600)$ and a background or that the ρ' consists of two overlapping 1^{-} states[24] which interfere. Existing data is inadequate to resolve between these possibilities.

REFERENCES

1) H.H. Bingham et al., Phys. Let. 41B (1972) 635.

2) D. Aston et al., Nucl. Phys. B189 (1981) 15.

3) B. Esposito et al., Lett. Nuovo Cimento 28 (1980) 195.

4) C. Bacci et al., Phys. Lett. 95B (1980) 139.

5) A. Cordier et al., Phys. Lett. 109B (1982) 129.

6) M. Atkinson et al., Phys. Lett. 108B (1982) 55.

7) M. Spinetti, Proc. Int. Symp. on Lepton and Photon Interactions (1979), 506.

8) M.S. Atiya et al., Phys. Rev. Lett. 43 (1979) 1691.

9) D. Aston et al., Phys. Lett. 92B (1980) 215.

10) D. Aston et al., Nucl. Phys. B174 (1980) 269.

11) G. Busetto and L. Oliver, Zeit. Phys. C 20 (1984) 247.

12) P. Gavillet et al., Phys. Lett. 69B (1977) 119.
C. Daum et al., Nucl. Phys. B182 (1982) 269.
J.A. Dankowych et al., Phys. Rev. Lett. 46 (1982) 580.

13) R. Aaron et al., Phys. Rev. D 24 (1981) 1207.
G. Bellini et al., CERN-EP/81-98 (1981).
M. Bonesini et al., Phys. Lett. 103B (1981) 75.
C. Daum et al., Nucl. Phys. B182 (1982) 269.

14) D. Aston et al., Nucl. Instrum. Methods 197 (1982) 287.

15) J.-C. Lassalle et al., Nucl. Instrum. Methods 176 (1980) 371.

16) M. Atkinson et al., CERN-EP/83-185 (1983) and Nucl. Phys. B (to be published).

17) SAGE, A general system for Monte Carlo event generation with preferred phase space density distributions, J. Friedman, UCRL Group A programming note, P-189 (1971).

18) C. Baltay et al., Phys. Rep. D17 (1978) 62.

19) G. Smadja et al., Proc. 1972 Philadelphia Conf. on Meson Spectroscopy, AIP, p. 349.

20) C. Zemach, Phys. Rev. 140B (1965) 97.

21) R.J. Cashmore, Multiparticle spectrometers and their use in meson spectroscopy, Invited talk, Daresbury Study Weekend Series, No. 8, DL/R34.

22) F. James and M. Roos, MINUIT, CCCPL Long write-up D506 (1977).

23) Particle Data Group, Phys. Lett. 111B (1982).

24) S. Godfrey and N. Isgur, Mesons with chromodynamics, University of Toronto Preprint, February (1984).

Figure captions

Fig. 1 : Layout of the detector.

Fig. 2 : a) Plot of difference in longitudinal momentum between initial and final states.
b) Plot of laboratory momentum of final state π^- for data (error bars) and Monte Carlo simulation (full line).
c) Plot of laboratory momentum of final state π^o for data (error bars) and Monte Carlo simulation (full line).

Fig. 3 : Plot of 4π mass spectrum:
a) Before ω exclusion; and
b) After ω exclusion.

Fig. 4 : Various mass spectra in the 4π mass range $1.4 < m_{\pi\pi} < 1.8$ GeV for data (error bars) and Monte Carlo simulation (full line):
a) $\pi^+\pi^-$ spectrum.
b) $\pi^\pm\pi^o$ spectrum.
c) $\pi^o\pi^o$ spectrum.
d) $\pi^+\pi^-\pi^o$ spectrum.
e) $\pi^\pm\pi^o\pi^o$ spectrum.

Fig. 5 : Definition of the $\pi^+\pi^-\pi^o\pi^o$ system, its angles and angular momenta, used in the model-independent analysis. θ_e is the angle of the π^+ in the ρ with respect to the ρ direction in the ρ' centre of mass. $\theta_{\pi\pi}$ is the angle of the π^o in the $\pi\pi$ system opposite the ρ with respect to the direction of the $\pi\pi$ system in the ρ' centre of mass.

Fig. 6 : Results of maximum likelihood fit to model-independent analysis. In this figure ℓ is the orbital angular momentum of the two π's opposite the e and L is the orbital angular momentum between the $\pi\pi$ system and the e:
a) $\ell = 0$, $L = 0$ intensity.
b) $\ell = 0$, $L = 1$ intensity.
c) $\ell = 1$, $L = 0$ intensity.
d) $\ell = 1$, $L = 1$ intensity.

e) $K_S K^{\pm}\pi^{\mp}$ background intensity.
f) $\pi^+\pi^-\pi^o\pi^o$ phase-space intensity.

Fig. 7 : Projections of model-independent maximum likelihood fit on the data for various spectra.
a) $\pi^+\pi^-$.
b) $\pi^{\pm}\pi^o$.
c) $\pi^o\pi^o$.
d) $\pi^+\pi^-\pi^o$.
e) $\pi^{\pm}\pi^o\pi^o$.

Fig. 8 : Results of maximum likelihood fit for model-dependent analysis. This figure shows the fitted intensities of the phase-space models:
a) $\rho^{\pm}\pi^{\mp}\pi^o$.
b) $\rho^+\rho^-$.
c) $\pi'^{\pm}\pi^{\mp}$.
d) $A_1^{\pm}\pi^{\mp}$.
e) $A_2^{\pm}\pi^{\mp}$.
f) $\rho^o\pi^o\pi^o$.
g) $H\pi$.
h) $K_S K^{\pm}\pi^{\mp}$ background.
i) $\pi^+\pi^-\pi^o\pi^o$.

Fig. 9 : a) Comparison of the shapes of the Monte Carlo mass spectra for the $A_1^{\pm}\pi^{\mp}$ (full line) and the $\rho^{\pm}\pi^{\mp}\pi^o$ (dotted line) phase-space models.

b) Comparison of the shapes of the Monte Carlo mass spectra for the $\rho^{\pm}\pi^{\mp}\pi^o$ SCHC (solid line) and the $\rho^{\pm}\pi^{\mp}\pi^o$ (dotted line) phase-space models.

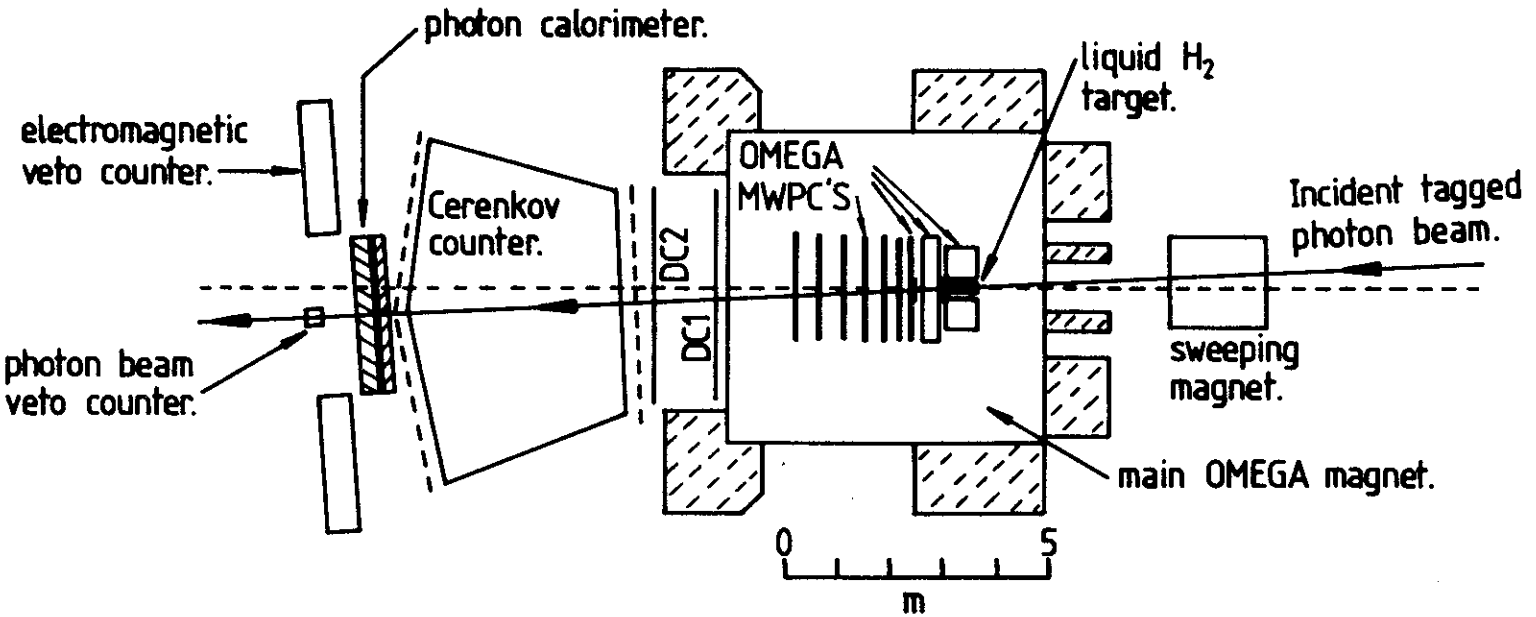
photon calorimeter.
liquid H_2 target.
electromagnetic veto counter.
OMEGA MWPC'S
Cerenkov counter.
DC2
DC1
Incident tagged photon beam.
photon beam veto counter.
sweeping magnet.
main OMEGA magnet.
0
5
m

Fig. 1.

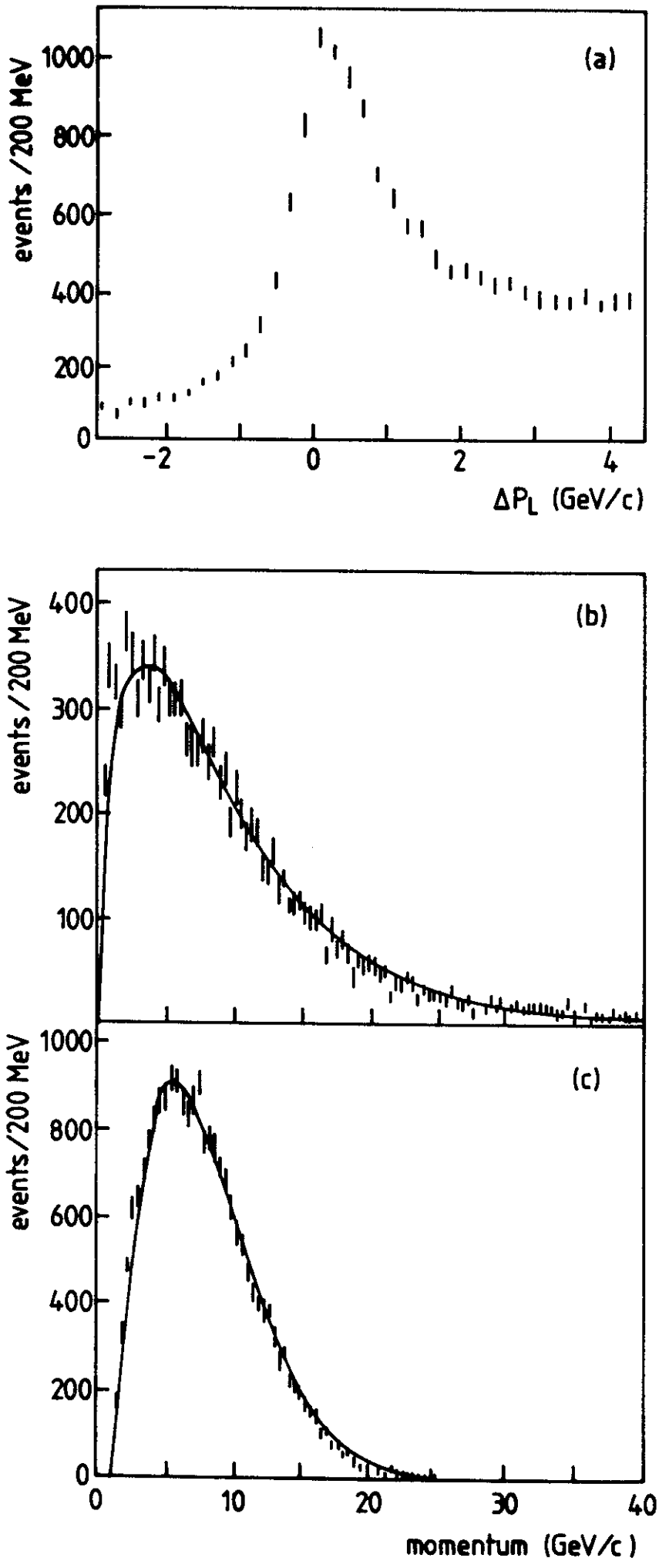
(a)
events / 200 MeV
1000
800
600
400
200
0
-2
0
2
4
ΔP_L (GeV/c)
(b)
events / 200 MeV
400
300
200
100
(c)
events / 200 MeV
1000
800
600
400
200
0
0
10
20
30
40
momentum (GeV/c)

Fig. 2.

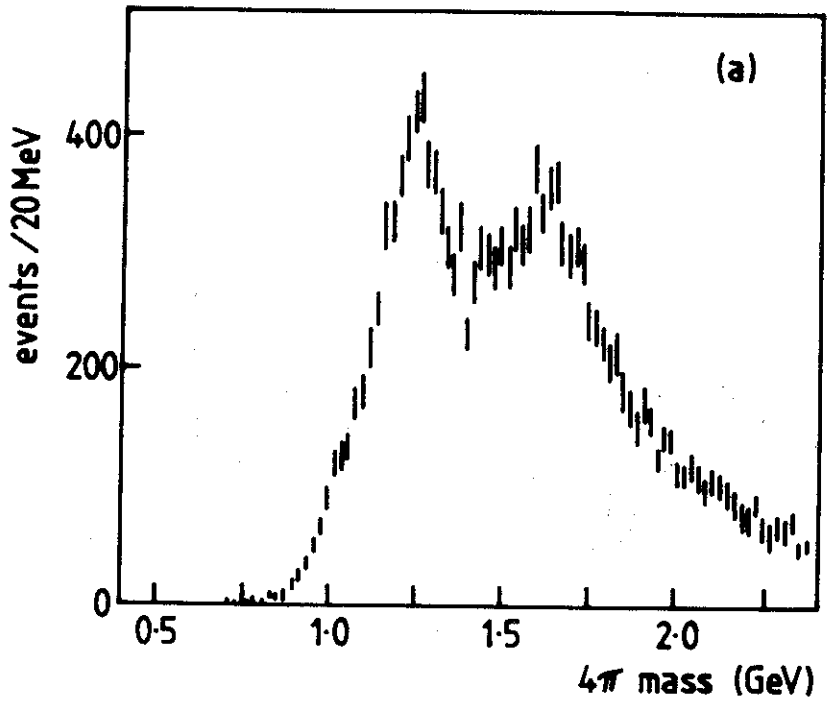
(a)
events /20 MeV
400
200
0
0·5
1·0
1·5
2·0
4π mass (GeV)

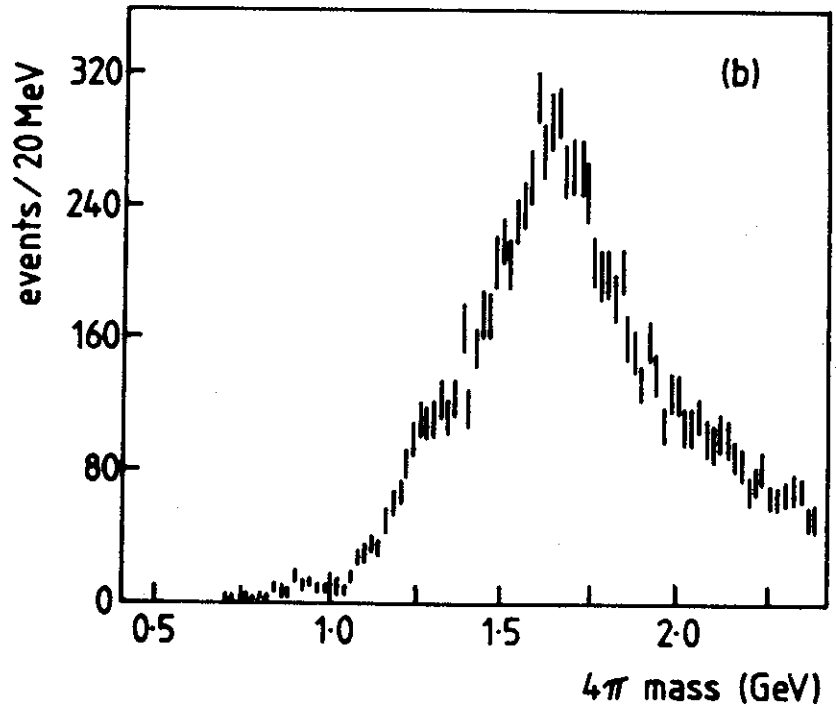
(b)
events / 20 MeV
320
240
160
80
0
0·5
1·0
1·5
2·0
4π mass (GeV)

Fig. 3.

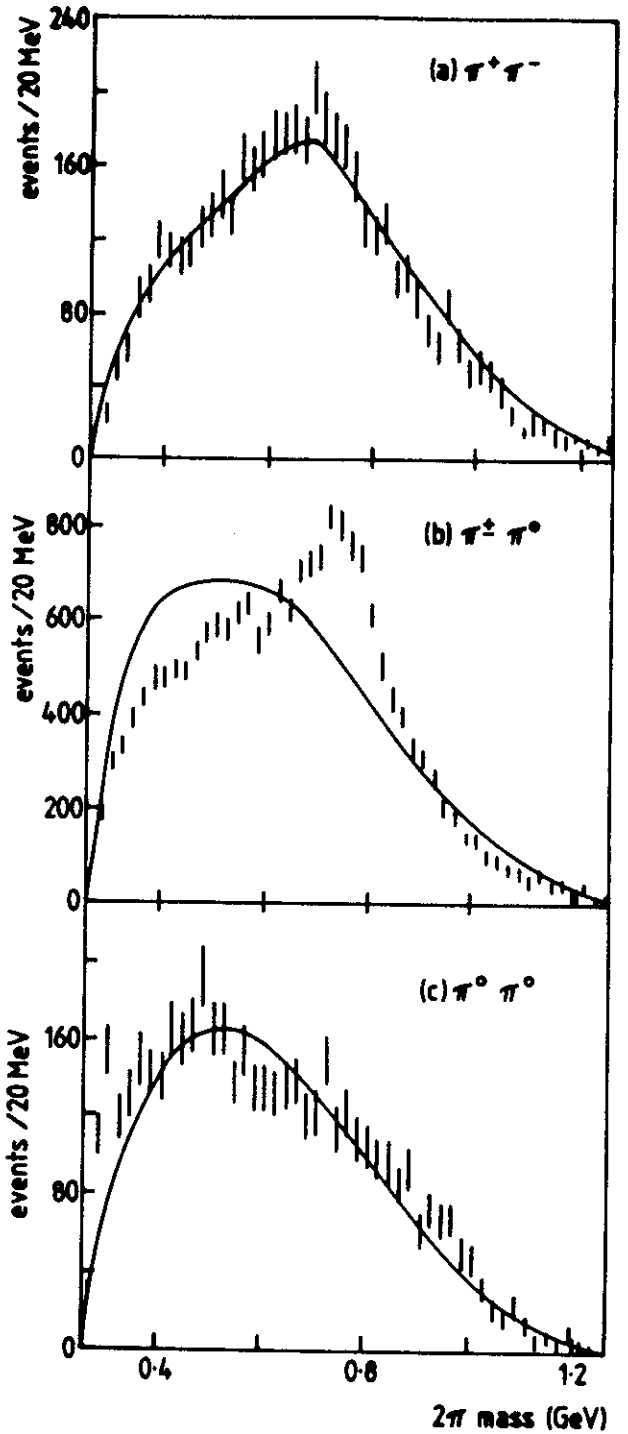
(a) $\pi^+\pi^-$
(b) $\pi^\pm\pi^0$
(c) $\pi^0\pi^0$
events / 20 MeV
0
80
160
240
200
400
600
800
0·4
0·8
1·2
2π mass (GeV)

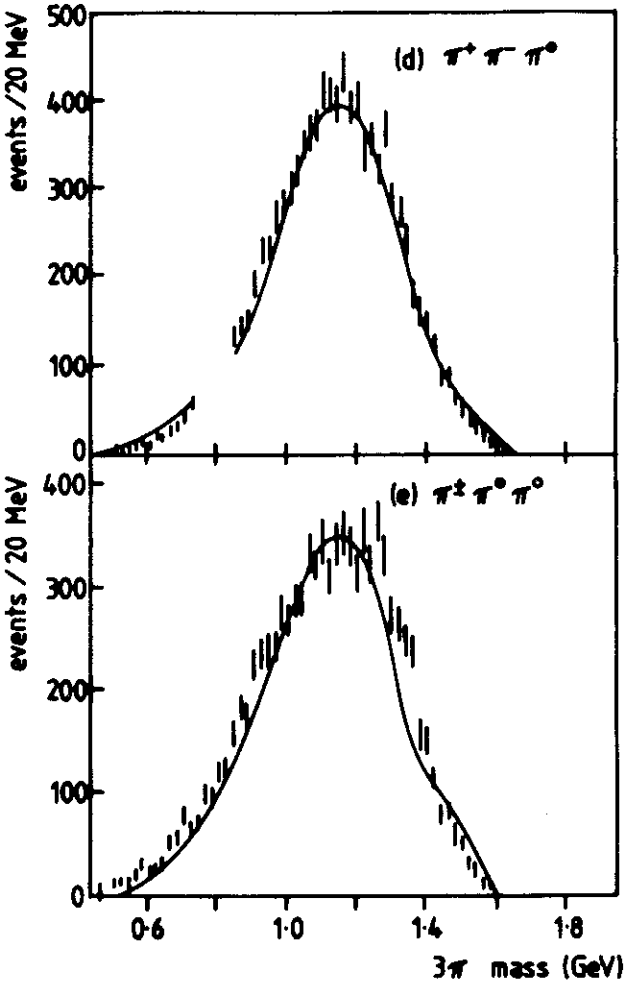
(d) $\pi^+\pi^-\pi^0$
(e) $\pi^\pm\pi^0\pi^0$
events / 20 MeV
0
100
200
300
400
500
0·6
1·0
1·4
1·8
3π mass (GeV)

Fig. 4.

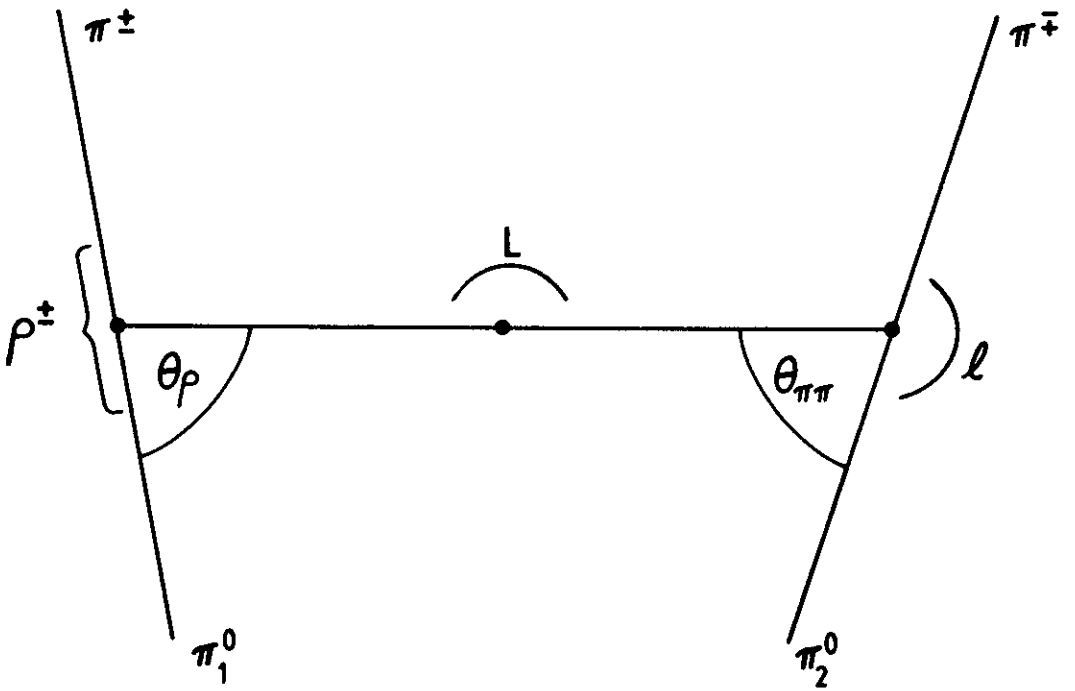

Fig. 5.

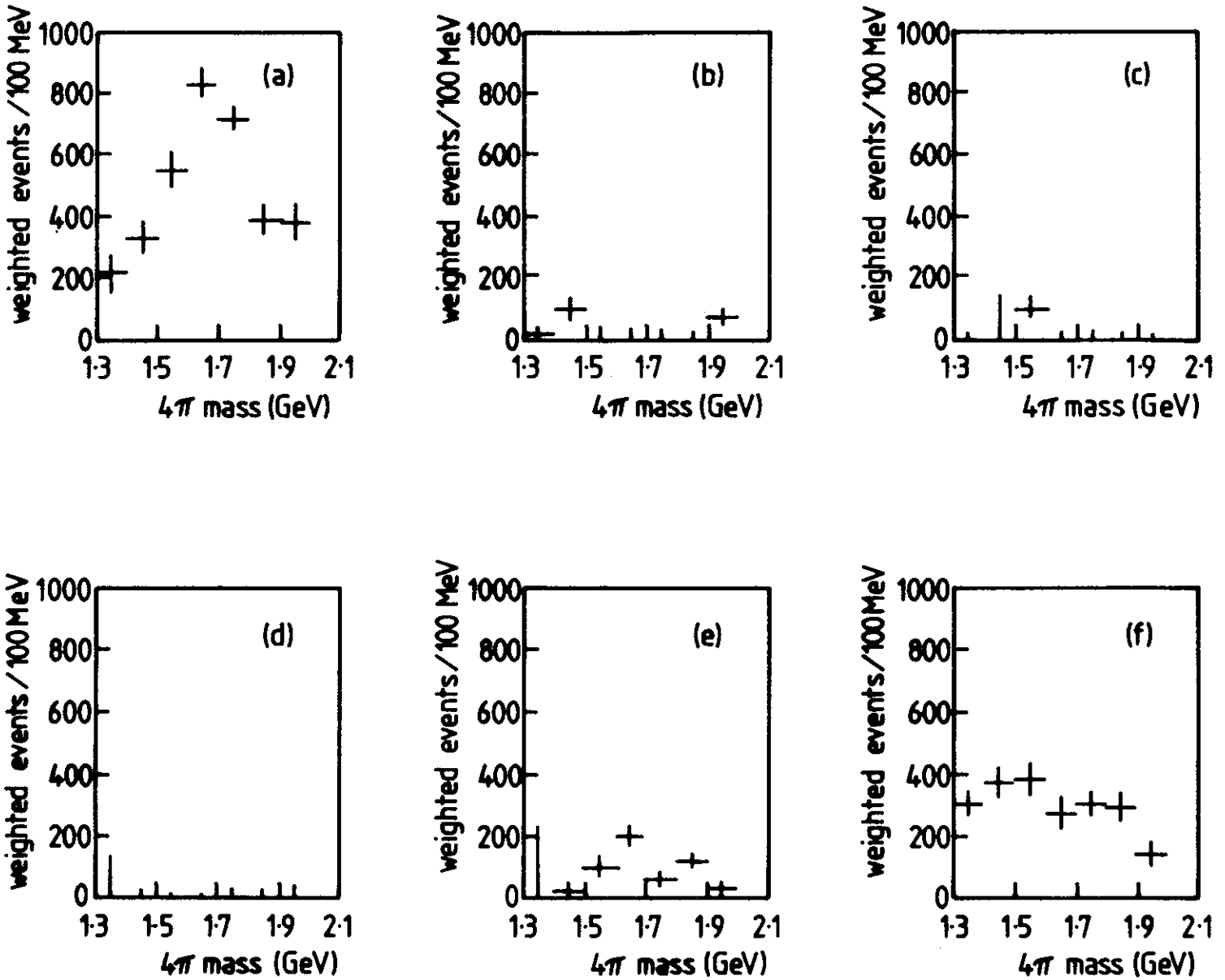
(a)
(b)
(c)
(d)
(e)
(f)
weighted events / 100 MeV
4π mass (GeV)
0
200
400
600
800
1000
1·3
1·5
1·7
1·9
2·1

Fig. 6.

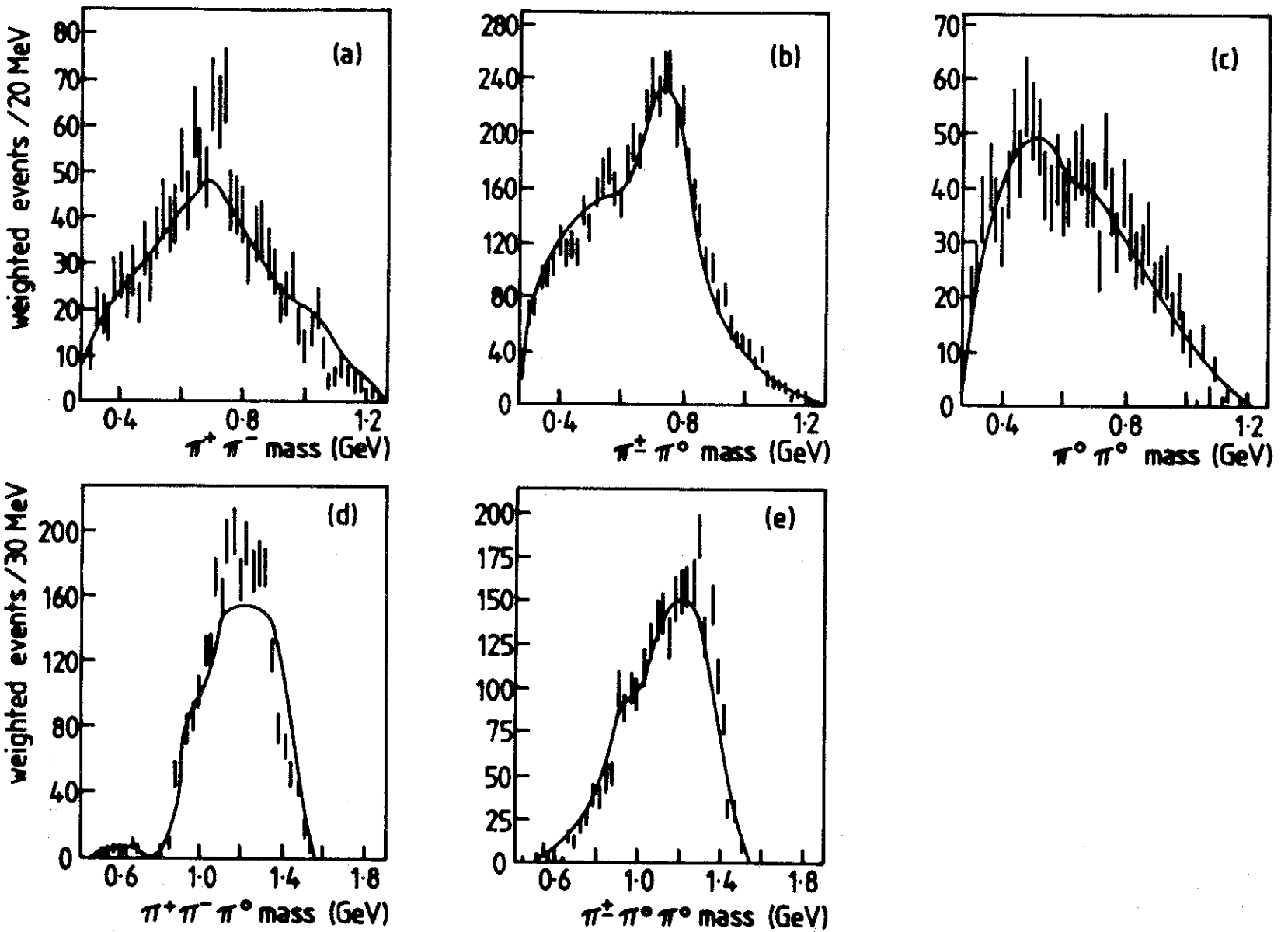
weighted events /20 MeV
(a)
$\pi^+\pi^-$ mass (GeV)
(b)
$\pi^\pm\pi^\circ$ mass (GeV)
(c)
$\pi^\circ\pi^\circ$ mass (GeV)
weighted events /30 MeV
(d)
$\pi^+\pi^-\pi^\circ$ mass (GeV)
(e)
$\pi^\pm\pi^\circ\pi^\circ$ mass (GeV)

Fig. 7.

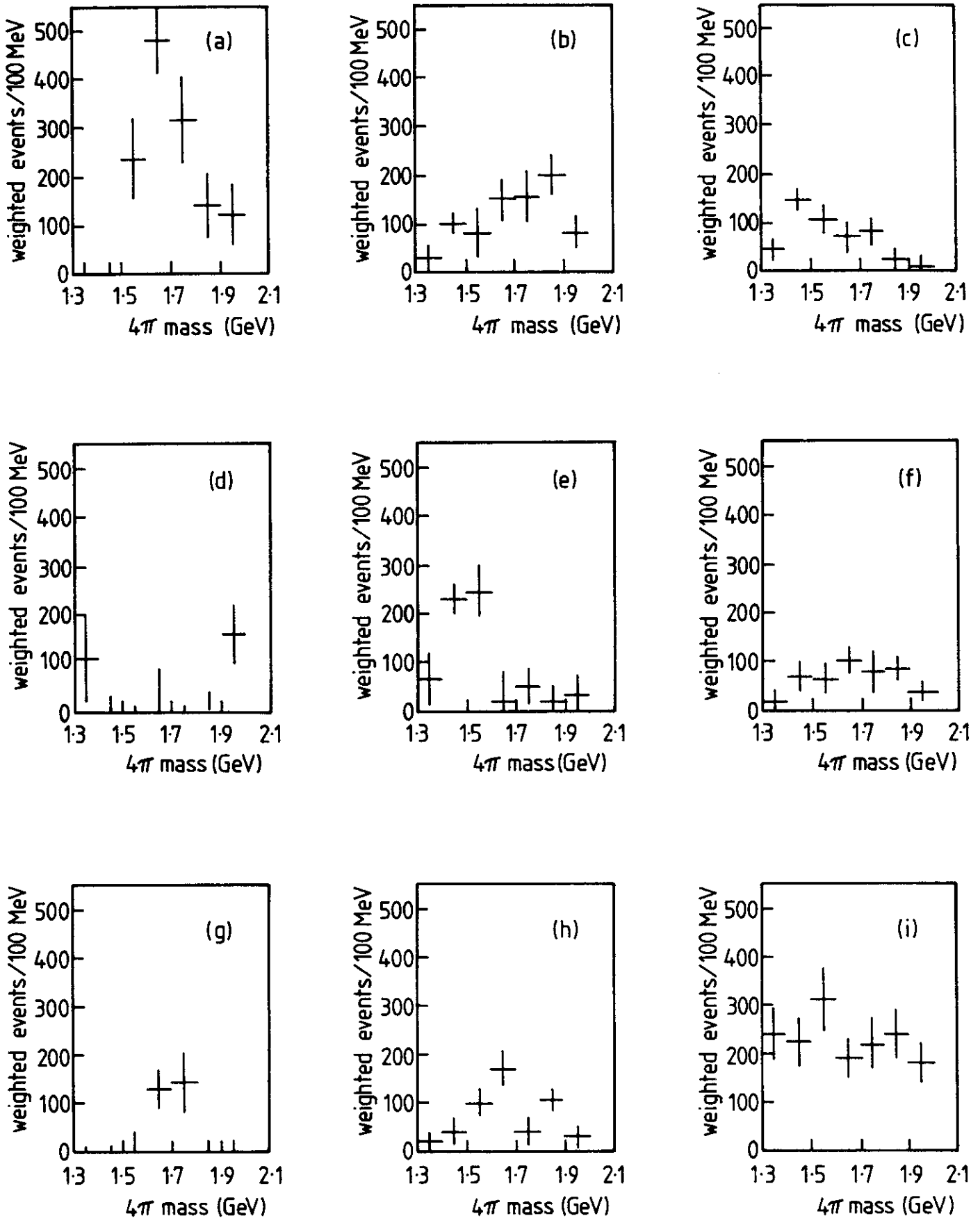
(a)
(b)
(c)
(d)
(e)
(f)
(g)
(h)
(i)
weighted events/100 MeV
0
100
200
300
400
500
1·3
1·5
1·7
1·9
2·1
4π mass (GeV)

Fig. 8.

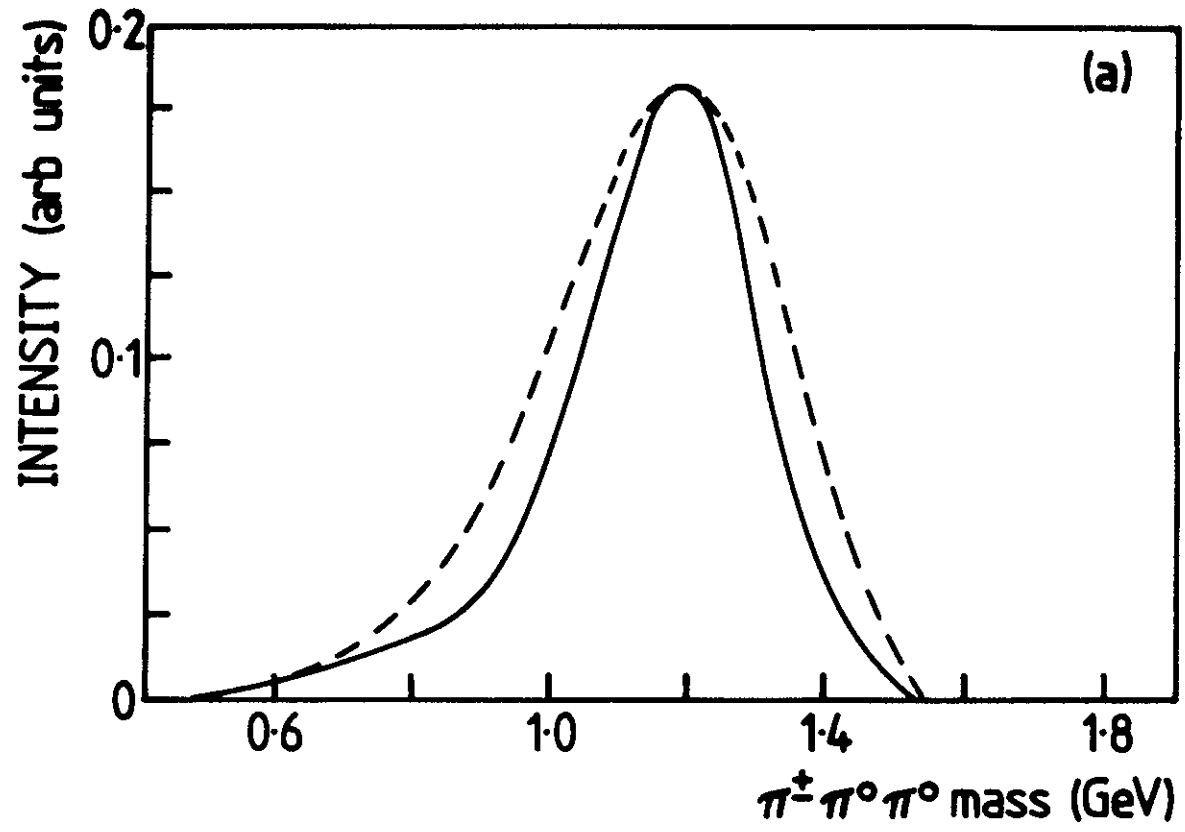
INTENSITY (arb units)
0·2
0·1
0
(a)
0·6
1·0
1·4
1·8
$\pi^{\pm}\pi^{\circ}\pi^{\circ}$ mass (GeV)

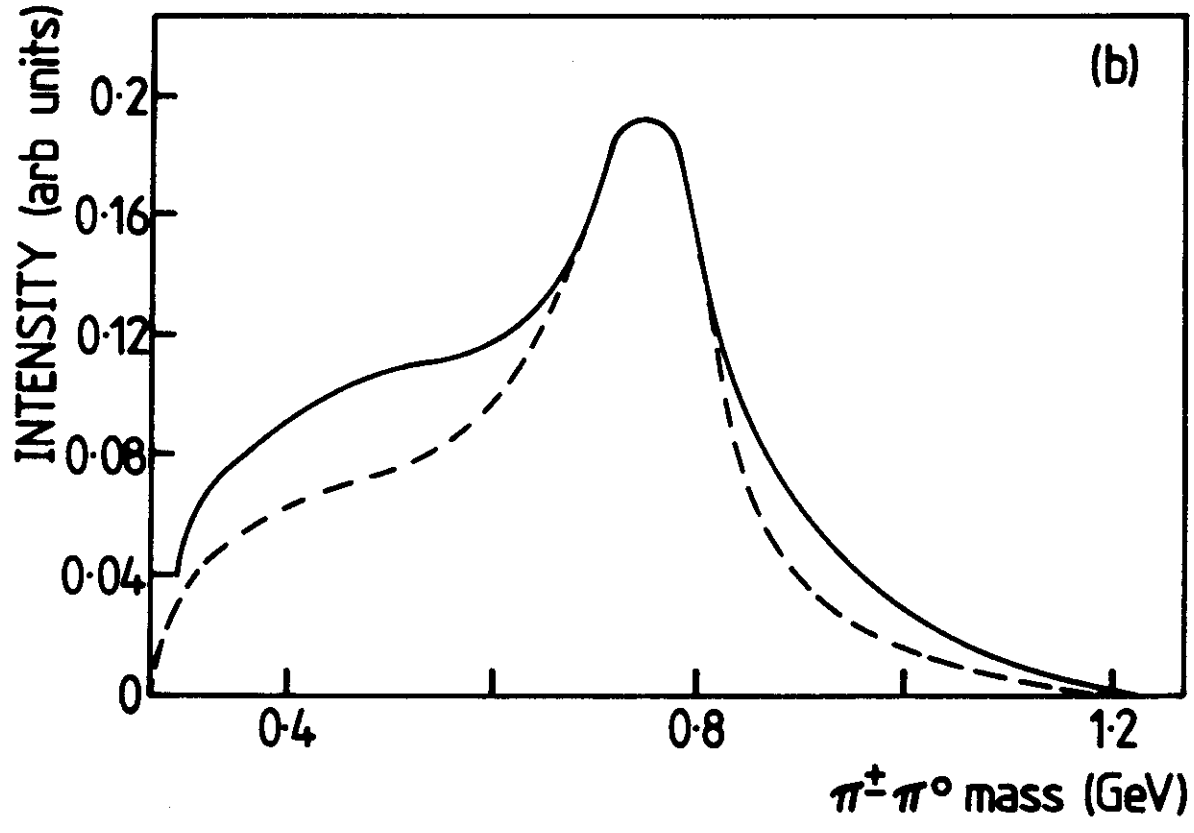
INTENSITY (arb units)
0·2
0·16
0·12
0·08
0·04
0
(b)
0·4
0·8
1·2
$\pi^{\pm}\pi^{\circ}$ mass (GeV)

Fig. 9.